Preclinical Evaluation of ^{18}F-JNJ64349311, a Novel PET Tracer for Tau Imaging

Lieven Declercq[1], Frederik Rombouts[2], Michel Koole[3], Katleen Fierens[4], Jonas Mariën[2], Xavier Langlois[2], José Ignacio Andrés[5], Mark Schmidt[6], Gregor Macdonald[2], Diederik Moechars[2], Wim Vanduffel[7], Thomas Tousseyn[8], Rik Vandenberghe[9], Koen Van Laere[3], Alfons Verbruggen[1], and Guy Bormans[1]

[1]Laboratory for Radiopharmacy, Department of Pharmaceutical and Pharmacological Sciences, KU Leuven, Leuven, Belgium; [2]Neuroscience Discovery, Janssen Research and Development, a division of Janssen Pharmaceutica NV, Beerse, Belgium; [3]Nuclear Medicine & Molecular Imaging, Department of Imaging and Pathology, KU Leuven and University Hospital Leuven, Leuven, Belgium; [4]Discovery Sciences, Janssen Research and Development, a division of Janssen Pharmaceutica NV, Beerse, Belgium; [5]Discovery Sciences, Janssen Research and Development, a division of Janssen-Cilag NV, Toledo, Spain; [6]Janssen Early Development, a division of Janssen Pharmaceutica NV, Beerse, Belgium; [7]Laboratory for Neuro- and Psychophysiology, Department of Neurosciences, KU Leuven, Leuven, Belgium; [8]Translational Cell & Tissue Research, Department of Imaging & Pathology, KU Leuven, Leuven, Belgium; and [9]Laboratory for Cognitive Neurology, Department of Neurosciences, KU Leuven, Leuven, Belgium

In this study, we have synthesized and evaluated ^{18}F-JNJ64349311, a tracer with high affinity for aggregated tau (inhibition constant value, 8 nM) and high (≥500×) in vitro selectivity for tau over β-amyloid, in comparison with the benchmark compound ^{18}F-AV1451 (^{18}F-T807) in mice, rats, and a rhesus monkey. **Methods:** In vitro binding characteristics were determined for Alzheimer's disease, progressive supranuclear palsy, and corticobasal degeneration patient brain tissue slices using autoradiography studies. Ex vivo biodistribution studies were performed in mice. Radiometabolites were quantified in the brain and plasma of mice and in the plasma of a rhesus monkey using high-performance liquid chromatography. Dynamic small-animal PET studies were performed in rats and a rhesus monkey to evaluate tracer pharmacokinetics in the brain. **Results:** Mouse biodistribution studies showed moderate initial brain uptake and rapid brain washout. Radiometabolite analyses after injection of ^{18}F-JNJ64349311 in mice showed the presence of a polar radiometabolite in plasma, but not in the brain. Semiquantitative autoradiography studies on postmortem tissue sections of human Alzheimer's disease brains showed highly displaceable binding to tau-rich regions. No specific binding was, however, found on human progressive supranuclear palsy and corticobasal degeneration brain slices. Small-animal PET scans of Wistar rats revealed moderate initial brain uptake (SUV, ~1.5 at 1 min after injection) and rapid brain washout. Gradual bone uptake was, however, also observed. Blocking and displacement did not affect brain time–activity curves, suggesting no off-target specific binding of the tracer in the healthy rat brain. A small-animal PET scan of a rhesus monkey revealed moderate initial brain uptake (SUV, 1.9 at 1 min after injection) with a rapid washout. In the monkey, no bone uptake was detected during the 120-min scan. **Conclusion:** This biologic evaluation suggests that ^{18}F-JNJ64349311 is a promising tau PET tracer candidate, with a favorable pharmacokinetic profile, as compared with ^{18}F-AV1451.

Key Words: Alzheimer's disease; progressive supranuclear palsy; corticobasal degeneration; tau; PET; biomarker; PHFs; brain; diagnostic; ^{18}F-JNJ64349311; ^{18}F-AV1451

J Nucl Med 2017; 58:975–981
DOI: 10.2967/jnumed.116.185199

Despite huge efforts over the last few decades, more than 99% of drug candidates tested against Alzheimer's disease (AD), aiming at slowing disease progression or symptomatic improvement, ultimately failed in late-stage-development clinical trials (*1*). The pharmacologic mechanism may simply not have been translated to therapeutic benefit in many cases; however, another major problem has been reliance on clinical diagnosis for subject selection. The availability of fluid and imaging biomarkers such as cerebrospinal fluid β-amyloid and PET using radioligands for β-amyloid plaques promises to greatly improve diagnosis, although there continues to be a need for biomarkers predictive of decline. Tau (tubulin-associated unit) protein markers gained increasing interest in the last years because of a close correlation of cerebral tau deposition with clinical symptoms in AD and other tauopathies (*2*). Indeed, the extent and distribution of tau deposition may be more specific to Alzheimer dementia and predictive of decline in subjects at risk for dementia, compared with β-amyloid plaque density in the brain (*3*). The design of tau PET ligands, however, has proven to be challenging, because of the complexity of tau as a PET target. Under pathologic conditions, tau is hyperphosphorylated, self-aggregates into paired helical filaments (PHFs), and eventually forms tangles that also contain other proteins. Because tau exists in six different isoforms, tau is subject to various posttranslational modifications, and tangles can have many ultrastructural conformations, the development of a specific tau PET tracer able to target tau pathology in AD remains daunting (*4*). Nonetheless, several tau-specific PET ligands have been developed in the past decade, and they were recently discussed in a review by Dani et al. (*5*). Among the first of these identified was T807, a tracer developed by Siemens and then licensed to Eli Lilly, now known

Received Nov. 3, 2016; revision accepted Feb. 3, 2017.
For correspondence or reprints contact: Diederik Moechars, Neuroscience Discovery, Janssen Research and Development, a division of Janssen Pharmaceutica NV, Turnhoutseweg 30, 2340 Beerse, Belgium.
E-mail: dmoechar@its.jnj.com
Published online Feb. 23, 2017.

as ^{18}F-AV1451. This tracer is the most widely studied, and the signal in the brain has been demonstrated to follow Braak stages in cross-sectional studies of subjects at risk for AD to full blown AD (*6*). However, it has some off-target binding (*7*) and exhibits a problematic kinetic profile, clearing slowly and failing to reach steady state in some brain regions (*8–11*). On the other hand, some reports demonstrated that ^{18}F-AV1451 may also have some affinity for non-AD tauopathies (*5*). The aim of the present study was to develop a tau PET ligand with a pharmacokinetic profile superior to that of ^{18}F-AV1451 but with similar or better affinity to and selectivity for β-amyloid plaque. We report here the in vitro and in vivo evaluation of ^{18}F-JNJ64349311 (^{18}F-JNJ311) by autoradiography studies on postmortem human AD, progressive supranuclear palsy (PSP), and corticobasal degeneration (CBD) brain slices, biodistribution and radiometabolite studies in mice, and small-animal PET studies in rats and a rhesus monkey, in comparison with ^{18}F-AV1451.

MATERIALS AND METHODS

Synthesis and evaluation of the authentic reference compound of JNJ311 (including precursor) were published in detail elsewhere (*12*), as well as the medicinal chemistry resulting in the discovery of this fluorinated compound. The precursor for radiosynthesis of ^{18}F-AV1451 and the authentic reference material and the nonradioactive reference material for AV680 and AV45 were synthesized by Janssen Research and Development (Janssen Pharmaceutica NV, Beerse, Belgium) according to literature reports (*13*). All other chemicals and reagents were purchased from commercial sources and used without further purification. The distribution coefficient ($LogD_{7.4}$) of JNJ311 was determined by Sirius Analytic Instruments according to a previously described report (*14*). The calculated polar surface area was obtained using MarvinSketch (version 6.1.0; ChemAxon). For analysis of radiolabeled compounds, the high-performance liquid chromatography (HPLC) column eluate, after passing through the ultraviolet detector, was led over a 7.62-cm NaI(Tl) scintillation detector connected to a single channel analyzer (GABI box; Raytest). Data were acquired and analyzed using a GINA Star data acquisition system (Raytest). Quantification of radioactivity in samples of biodistribution and radiometabolite studies was performed according to a previously reported procedure (*13*). Quantitative data are expressed as mean ± SD. Means were compared using an unpaired 2-tailed Student *t* test. Values were considered statistically significant for a *P* value of 0.05 or less. Postmortem human AD brain slices were provided by University Hospitals Leuven (10-μm thick; Neurology Department), after approval from the local Institutional Review Board. Postmortem human CBD and PSP brain slices were provided by Janssen Research and Development (10-μm thick; Neuroscience Biology Department, Belgium), after approval from the Use Committee of Janssen Pharmaceutical Companies of Johnson & Johnson and the local ethical committee. Animals were housed in individually ventilated cages in a thermoregulated (~22°C), humidity-controlled facility under a 12 h–12 h light–dark cycle, with access to food and water ad libitum. All animal experiments were conducted according to the Belgian code of practice for the care and the use of animals, after approval from the university animal ethics committee.

Radiosynthesis

^{18}F-fluoride ($^{18}F^-$) was produced and purified according to a previously described procedure (*13*). A solution of 0.5 mg of trimethylammonium precursor (mono- or tris-trifluoroacetate salts) in 0.3 mL of dimethylformamide was added to the dried $^{18}F^-/K_2CO_3$/K-222 residue, and the mixture was heated at 120°C for 10 min. The crude radiolabeling mixture was diluted with a 0.6-mL mobile phase and purified using reversed-phase HPLC on an XBridge C_{18} column (5 μm, 4.6 × 150 mm; Waters) eluted with a mixture of 0.01 M Na_2HPO_4, pH 9.6, and EtOH (65:35 v/v) at a flow rate of 0.8 mL/min and with ultraviolet detection at 254 nm. The purified radiotracer solution was diluted with saline to obtain an ethanol concentration less than 10%, suitable for intravenous injection. The solution was subsequently passed through a 0.22-μm filter (Millex-GV; Millipore) to obtain a sterile product. Quality control was performed using reversed-phase HPLC on an XBridge column (C_{18}, 3.5 μm, 3.0 × 100 mm; Waters) eluted with a mixture of 0.01 M Na_2HPO_4, pH 9.6, and CH_3CN (70:30 v/v) at a flow rate of 0.8 mL/min. Ultraviolet detection was performed at 254 nm. ^{18}F-AV1451 was radiolabeled according to a previously reported procedure (*13*).

Biodistribution Studies

Biodistribution studies were performed in healthy male Naval Medical Research Institute (NMRI) mice (body weight, 30–40 g) at 2, 10, 30, and 60 min after injection (n = 3/time point) according to a previously reported procedure (*13*). SUVs were calculated as (counts per minute in body part/weight of the body part in g)/(sum of counts per minute in all body parts/body weight in g).

Autoradiography Studies

Air-dried frozen, 10-μm-thick postmortem slices of an AD patient (visual cortex of a 68-y-old woman with Braak stage VI), PSP patient (frontal cortex of a 71-y-old woman), and CBD patient (frontal cortex of a 74-y-old woman) were incubated for 60 min in a solution of tracer (740 kBq/500 μL per section) and subsequently washed with mixtures of phosphate-buffered saline and ethanol as described elsewhere (*15*). To assess specificity of binding, slices were incubated with radiotracer in the presence of 1 μM of authentic reference compound, AV680 or AV45 (the latter 2 compounds were used only on the AD brain slices). After being dried, slices were exposed to a phosphor storage screen (super-resolution screen; Perkin Elmer). Screens were read in a Cyclone Plus system (Perkin Elmer) and analyzed using Optiquant software. Results are expressed as digital light units per square mm (digital light units/mm^2).

Phosphorylated PHF Tau and β-Amyloid Plaque Isolation from Human AD Brain

Enriched PHF tau and β-amyloid plaque fractions were prepared as previously described (*13*), using postmortem human AD brain tissue with high tau fibril or high β-amyloid plaque load, respectively.

In Vitro Competitive Radioligand Binding Assays

The competitive radioligand binding assays measured the binding of a fixed amount of ^{3}H-AV680 (PHF tau binder) or ^{3}H-AV45 (β-amyloid plaque binder) in the presence of a concentration range of test compounds following a described experimental assay setup (*13*).

Immunohistochemistry

Adjacent AD, PSP, or CBD slices were used for immunohistochemistry to correlate with radiotracer binding. Sections were first dried, fixed in 4% formaldehyde, treated for 5 min with hydrogen peroxide (5%; S2023 [DAKO]), and permeabilized with phosphate buffer containing 0.3% Triton X-100 (Thermo Fisher), followed by a 1-h incubation immunostaining with antitau (AT8, in-house made; 0.4 μg/mL) or anti-β-amyloid antibodies (4G8, 2 μg/mL [Eurogentec] SIG-39200) in the AD case. After extensive washing, slices were incubated for 30 min with horseradish peroxidase–conjugated anti-mouse secondary antibody (DAKO, K4000; Envision), followed by chromogenic 3,3-diaminobenzidine labeling (K3468; DAKO). Finally, sections were counterstained with hematoxylin, dehydrated, and mounted with permanent mounting medium (Vectamount H-5000; Vector Laboratories).

Radiometabolite Studies

Perfused Brain Radiometabolites. The study was performed in NMRI mice at 10 or 60 min after injection ($n = 3$/time point) according to a previously described procedure (*13*). HPLC analysis was performed on a C_{18} column (XBridge 3.5 μm, 3.0 × 100 mm; Waters) eluted with a mixture of 0.01 M Na_2HPO_4, pH 9.6, and CH_3CN (77:23 v/v) at a flow rate of 0.7 mL/min.

Plasma Radiometabolites in Mice. NMRI mice were anesthetized with isoflurane (2.5% in O_2 at 1 L/min flow rate) and injected with ^{18}F-JNJ311 (~3.7 MBq) via a lateral tail vein. Mice were sacrificed by decapitation at 2, 10, 30, or 60 min after injection ($n = 3$/time point). Blood was collected in ethylenediaminetetraacetic acid–containing tubes (4-mL tubes; BD vacutainer [BD]), weighed, counted for radioactivity in the γ-counter, and stored on ice. Blood was subsequently centrifuged at 2,330*g* for 10 min to separate the plasma. Plasma (0.5 mL) was weighed, counted for radioactivity in a γ-counter, and spiked with 20 μg of authentic JNJ311. Afterward, proteins in the plasma sample were precipitated by adding an equal volume of CH_3CN followed by centrifugation for 5 min at 2,330*g*. Next, supernatant (0.5 mL) was collected, diluted with H_2O (0.7 mL), and filtered through a 0.22-μm filter (Nylon Acrodisc, 13 mm syringe filter; Pall Life Sciences). The sample was counted for radioactivity in the γ-counter before being analyzed by HPLC (Waters XBridge C_{18} column, 3.5 μm, 3.0 × 100 mm; eluted with a mixture of 0.01 M Na_2HPO_4, pH 9.6, and CH_3CN [77:23 v/v] at a flow rate of 0.7 mL/min). Ultraviolet detection was done at 254 nm. The HPLC eluate was collected as 1-mL fractions, and radioactivity of the fractions was counted in an automated γ-counter.

Small-Animal PET Imaging Studies

Wistar Rats. Dynamic 120-min small-animal PET scans with all tracers were acquired on a Focus 220 small-animal PET scanner (Concorde Microsystems) for three female Wistar rats simultaneously, which were scanned three times. The rats were kept under gas anesthesia during the whole procedure (2.5% isoflurane in O_2 at 1 L/min flow rate). Scans were acquired in list-mode, and acquisition data were Fourier-rebinned in 27 time frames (4 × 15, 4 × 60, 5 × 180, 8 × 300, and 6 × 600 s). Data, which were reconstructed using a 3-dimensional maximum a posteriori reconstruction, were manually aligned with a rat brain ^{18}F-FDG template in Paxinos coordinates using an affine transformation, to allow predefined volume-of-interest analysis (*16*). Time–activity curves of the whole brain were generated using volume-of-interest analysis with PMOD software (version 3.2; PMOD Technologies). Radioactivity concentration in the brain was expressed as SUV (calculated as [radioactivity in Bq in brain/mL]/[total injected dose [Bq]/body weight in g]) as a function of time after tracer injection. Scans were started immediately after intravenous injection of about 50 MBq of radiotracer. For pretreatment and displacement studies, solutions of cold reference compounds JNJ311 or AV1451 dissolved in a mixture of 5% dimethyl sulfoxide, 5% polysorbate 80, and 40% (2-hydroxypropyl)-β-cyclodextrin, filtered through a 0.22-μm membrane filter (Millex-GV; Millipore), were used. Pretreatment ($n = 3$) was done by subcutaneous injection of JNJ311 or AV1451 (10 mg/kg), 60 min before radiotracer injection. Displacement ($n = 3$) was performed by intravenous injection of JNJ311 or AV1451 (1 mg/kg) 30 min after radiotracer injection. Small-animal PET images were compared with a baseline scan ($n = 3$), acquired in a nontreated rat. A vehicle control study with ^{18}F-AV1451 was performed to assess the possible influence of the vehicle during the pretreatment and displacement study.

Rhesus Monkey. A dynamic 120-min small-animal PET scan with ^{18}F-JNJ311 or ^{18}F-AV1451 was obtained with a Focus 220 small-animal PET scanner on a male rhesus monkey (6-y-old *Macaca mulatta*, 7.6 kg) that was sedated with ketamine (Ketalar; Pfizer) and xylazine (Rompun; Bayer) via intramuscular injection. During scanning, the monkey received repeatedly an additional dose of ketamine/xylazine via intravenous injection. O_2 saturation in blood, breathing frequency, and heartbeat frequency were monitored during the entire experiment. The head of the animal was placed central in the field of view of the small-animal PET scanner. Scans were acquired in list-mode and Fourier-rebinned in 27 time frames (4 × 15, 4 × 60, 5 × 180, 8 × 300, and 6 × 600 s). Data were reconstructed using a 3-dimensional maximum a posteriori iterative reconstruction. Time–activity curves of the whole brain were generated using volume-of-interest analysis with PMOD software. Radioactivity concentration in the brain was expressed as SUV as a function of time after tracer injection. Scans were started immediately after intravenous injection of 185 MBq of ^{18}F-JNJ311 or ^{18}F-AV1451 via the vena saphena of the right leg. Blood samples were collected at 10, 30, and 60 min after injection via a catheter in the vena saphena of the left leg, and plasma was analyzed for radiometabolites according to the same procedure as for mice.

RESULTS

Human Pharmacokinetics (PK) Predictions for JNJ311

A human PK prediction was made on the basis of mouse, rat, and dog PK study (0.25 mg/kg, intravenously). The results are summarized in Supplemental Table 1 (supplemental materials are available at http://jnm.snmjournals.org). With the use of the Dedrick approach, a biphasic clearance in humans was predicted in which a fast clearance of 1.05 mL/min/kg was expected for the initial phase, resulting in a short half-life of 0.7 h (*17*). With allometric scaling, a high but slightly slower monophasic clearance of 1.285 mL/min/kg was predicted for humans, corresponding to a half-life of 2.4 h. Both models hence predicted JNJ311 to have a sufficiently fast clearance in humans after intravenous dosing, based on mouse, rat, and dog pharmacokinetic data after intravenous administration.

Radiolabeling

^{18}F-JNJ311 (Fig. 1) was synthesized by a nucleophilic substitution reaction with ^{18}F-fluoride on its trimethylammonium precursor. Heating of the precursor solution with ^{18}F-fluoride in the presence of K-222/K_2CO_3 afforded ^{18}F-JNJ311 ($n = 6$), with an average, decay-corrected, radiochemical yield of 46% (relative to total radioactivity of ^{18}F in the preparative chromatogram). Radiochemical yields were identical for the mono- and tris-trifluoroacetate salt of the precursor of ^{18}F-JNJ311. The radiochemical purity was more than 98%. ^{18}F-JNJ311 was obtained within a total synthesis time of 60 min. The specific activity of ^{18}F-JNJ311 was 81 ± 72 GBq/μmol at the end of synthesis. ^{18}F-AV1451 was collected within a total synthesis time of 60 min with a specific activity of 45 ± 35 GBq/μmol at the end of synthesis ($n = 4$) and a radiochemical purity greater than 95%.

Mouse Biodistribution Studies

Supplemental Table 2 shows SUVs of ^{18}F-JNJ311 and ^{18}F-AV1451 in different organs at 2, 10, 30, and 60 min after injection. High SUVs were recorded for the liver and kidneys, due to the hepatobiliary and renal plasma clearance of both compounds. Radioactivity concentration in blood decreased rapidly over time for ^{18}F-JNJ311 and ^{18}F-AV1451 (SUVs of, respectively, 0.5 and 0.4 at 2 min after injection, and this cleared to 0.1 and 0.2 by 60 min after injection). Rapid and moderate initial brain uptake was recorded, with an SUV of, respectively, 1.9 and 2.2 for ^{18}F-JNJ311 and ^{18}F-AV1451 at 2 min after injection. Brain washout was comparable for ^{18}F-JNJ311 and ^{18}F-AV1451, with SUVs around 0.1 at 60 min after injection ^{18}F-JNJ311 showed the highest

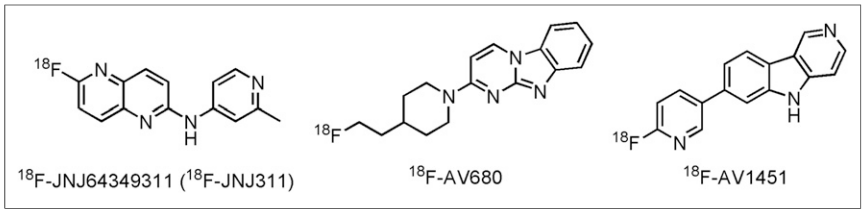

FIGURE 1. Chemical structures of ^{18}F-JNJ311, ^{18}F-AV1451, and ^{18}F-AV680.

2- to 60-min brain radioactivity ratio (29.6), whereas ^{18}F-AV1451 had a lower 2- to 60-min brain ratio (18.3, $P < 0.05$). Bone uptake was minimal and remained stable over time for both tracers.

In Vitro Autoradiography Binding Studies

Digital autoradiography with ^{18}F-JNJ311 on postmortem human AD brain slices showed binding to tau pathology–rich regions in the visual cortex (Fig. 2). No specific binding to tau pathology was, however, seen in the frontal cortex on the postmortem human PSP and CBD brain slices (Supplemental Fig. 1). Immunohistochemistry with tau and β-amyloid antibodies, performed on adjacent slices, identified numerous PHF and neuritic plaque deposits, confirming colocalization of tracer binding with PHFs in AD (Supplemental Fig. 2) but not in the PSP or CBD brain slices (Supplemental Fig. 3). To assess the specificity of the tracer binding to PHFs, blocking studies with authentic JNJ311, AV45, or AV680 were performed. Self-block studies with 1 μM of cold JNJ311 resulted in 90% inhibition ($n = 3$) in the AD brain slices, but only 14% and 10% inhibition ($n = 3$) in, respectively, the PSP and CBD brain slices. Binding of ^{18}F-JNJ311 was reduced, with 96% in the presence of 1 μM AV680 compared with control ($n = 3$) in the AD brain slices. Blocking of ^{18}F-JNJ311, on the other hand, with 1 μM of AV45 led to a blocking percentage of only 7% ($n = 3$) in the AD brain slices. Blocking percentages were calculated as (digital light units/mm^2 in the presence of 1 μmol/L blocker)/(digital light units/mm^2 tracer only).

In Vitro Competitive Radioligand Binding Assays

Binding assays with ^{3}H-AV680 in the presence of the cold test compounds showed high affinity of JNJ311 for enriched aggregated tau from human AD brain samples with an inhibition constant (K_i) value of 8 nM (Supplemental Table 3). In the competition assays with ^{3}H-AV45, only AV1451 and AV45 showed specific binding with a K_i value of 278 and 12 nM, respectively. JNJ311 and AV680 on the other hand, had K_i values higher than 4,398 nM.

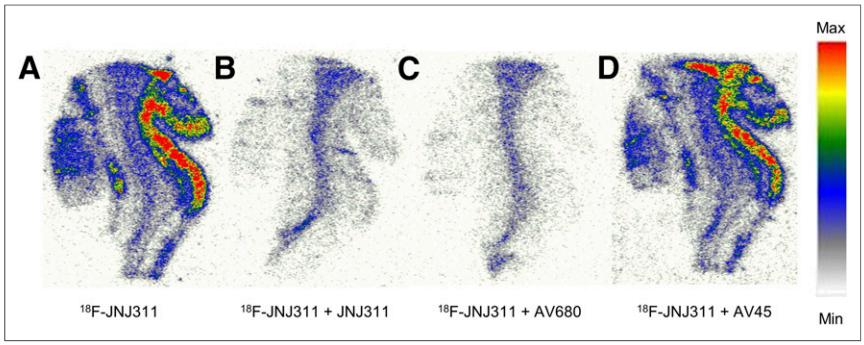

FIGURE 2. Adjacent, 10-μm-thick, postmortem human AD brain slices of visual cortex of AD patient (68-y-old with Braak stage VI) incubated with ^{18}F-JNJ311 (740 kBq/500 μL/slice) (A) in presence of authentic reference compound JNJ311 (B), AV680 (C), or AV45 (D) at 1 μmol/L.

Radiometabolites

Plasma radiometabolite analysis after intravenous administration of ^{18}F-JNJ311 in NMRI mice and a rhesus monkey revealed fast radiotracer metabolism. Thirty minutes after injection, 22% and 35% of the recovered radioactivity corresponded to intact tracer in mice and the rhesus monkey, respectively (Supplemental Table 4). All detected radiometabolites were more polar than the intact tracer at 60 min after injection. The recovery of the HPLC column-injected radioactivity for ^{18}F-JNJ311 was 95% for mice ($n = 12$) and 90% for the rhesus monkey ($n = 3$). In the brain, the percentage of intact ^{18}F-JNJ311 remained close to 100% at both 10 and 60 min after injection (Supplemental Table 4). The recovery of the HPLC column-injected radioactivity for ^{18}F-JNJ311 in brain extract was 90% ($n = 6$).

Small-Animal PET Imaging Studies

Wistar Rats. Results of the 120-min baseline, pretreatment, and displacement study are shown in Figure 3. Time–activity curves of the baseline scans of both ^{18}F-JNJ311 and ^{18}F-AV1451 show moderate initial brain uptake, with a comparably moderate SUV in the brain of about 1.5 at 1 min after injection. ^{18}F-JNJ311 had the fastest brain washout rate (SUV of 0.2 ± 0.04 at 60 min after injection) as shown in the %SUV$_{max}$ curves (Supplemental Fig. 4). Bone uptake was observed for both compounds at later time points, most likely due to defluorination (Fig. 3). No self-blocking or self-displacement effect was observed for ^{18}F-JNJ311 ($P >$ 0.05 at all time points), indicating absence of specific not tau-related binding in brain. Lower brain uptake of ^{18}F-AV1451 during the baseline scan, compared with the pretreatment study, was observed ($P < 0.05$ at 5 min after injection). An increase of brain activity was also observed after injection of a displacement dose at 30 min after injection for ^{18}F-AV1451 ($P < 0.05$ at 38 min after injection). No such differences were, however, recorded during a vehicle control study with ^{18}F-AV1451 (Supplemental Fig. 5).

Rhesus Monkey. Results of the 120-min baseline scan of ^{18}F-JNJ311 and ^{18}F-AV1451 are shown in Figure 4. Time–activity curves of the baseline scan of ^{18}F-JNJ311 in the brain show a fast, moderate initial brain uptake with a rapid washout (SUV of 1.9; time to peak, 1 min), and low white matter binding was recorded. Time–activity curves of the baseline scan of ^{18}F-AV1451 in the brain show a slower initial brain uptake (SUV of ~1.3; time to peak uptake, 15 min) and washout (Supplemental Fig. 6). Time–activity curves of the skull show that the SUV signal did not increase as a function of time for both compounds.

DISCUSSION

The aim of this study was the development of a selective aggregated ^{18}F-labeled tau PET ligand, with fast clearance from the brain. The medicinal chemistry optimization that resulted in the selection of JNJ311 as the best tau PET candidate (based on in vitro and in vivo data) was published elsewhere (*12*). In the present study, we describe the preclinical evaluation of this tau PET ligand, in comparison

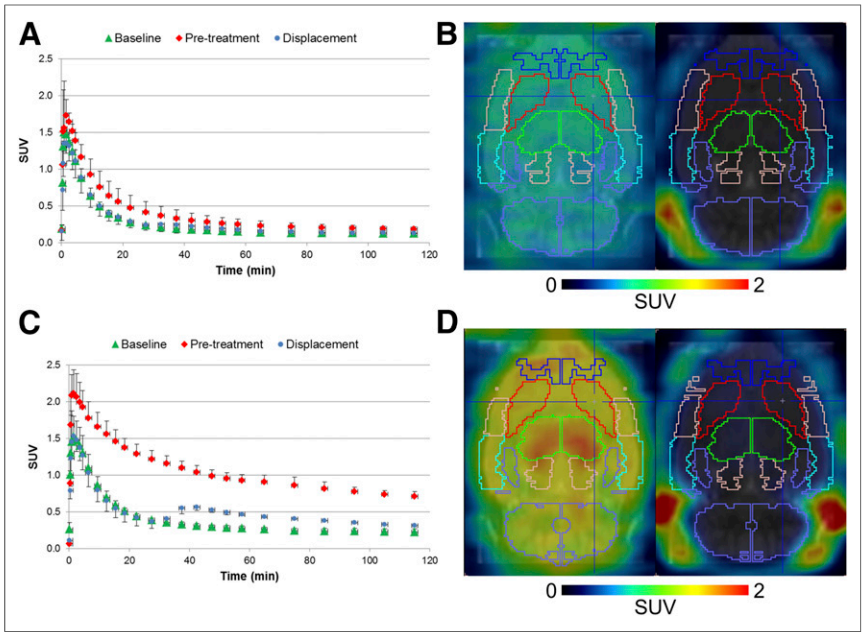

FIGURE 3. Whole-brain small-animal PET time–activity curves for ^{18}F-JNJ311 (A) and ^{18}F-AV1451 (C) of 3 female Wistar rats. Baseline scan (n = 3 per tracer); pretreatment experiment (n = 3 per tracer): cold JNJ311 (A and B) or AV1451 (C and D), 10 mg/kg injected subcutaneously 60 min before radiotracer injection; and displacement study (n = 3 per tracer): cold JNJ311 (A and B) or AV1451 (C and D), 1 mg/kg injected intravenously 30 min after radiotracer injection. Error bars correspond to SD. Representative transversal images of baseline experiment with ^{18}F-JNJ311 (B) and ^{18}F-AV1451 (D): averaged image 1–11 min after baseline tracer injection (left) and 90–120 min after tracer injection (right).

with ^{18}F-AV1451. JNJ311 was selected on the basis of its high affinity for aggregated tau (K_i value, 8 nM) and high specificity for tau over β-amyloid (more than 500× selective). JNJ311 was radiolabeled with ^{18}F, and the resulting radiotracer was evaluated in mice, rats, and rhesus monkey. Semiquantitative autoradiography experiments were used to evaluate binding characteristics in human AD, PSP, and CBD pathology. Such autoradiography studies are needed to determine the affinity for tau pathology in its natural AD, PSP, or CBD environment. 3R tauopathies, such as Pick disease, were not tested in this stage of tracer development, because of the low prevalence of tau inclusions in frontotemporal dementia (*18*). Results revealed high and selective binding to tau pathology in postmortem slices of the visual cortex for ^{18}F-JNJ311 in an AD patient in the latest Braak stage. No specific binding, on the other hand, could be demonstrated in the case of PSP or CBD pathology. To assess the specificity of the tracer binding to the tau pathology, self-blocking studies with the authentic reference compound JNJ311 and, in the AD case, also blocking studies with the structurally unrelated tau ligand AV680 and the specific β-amyloid ligand AV45 were performed. AV680 was used as the benchmark compound in this experiment, because of its higher selectivity for aggregated tau over β-amyloid and lower off-target binding than AV1451 (*19*). AV45 was used in the blocking studies to assess the specificity of JNJ311 for tau over β-amyloid. Self-block resulted in 90% inhibition in the cortical layers, demonstrating that the binding of ^{18}F-JNJ311 was specific. No specific binding could, however, be demonstrated in the frontal cortex of, respectively, PSP and CBD. Binding of ^{18}F-JNJ311 was also reduced with more than 79% in the presence of 1 μM AV680 on the AD brain slices, indicating tau-specific binding. Finally, blocking with AV45 resulted in only 7% displacement of ^{18}F-JNJ311, confirming that JNJ311 binds more selectively to tau pathology in the AD brain slices. Furthermore, immunohistochemistry performed on adjacent slices identified numerous hyperphosphorylated tau and neuritic plaque deposits in the cortical layers, with a pattern that, in the case of AD, visually correlated with the autoradiographic images, confirming colocalization of tracer binding with hyperphosphorylated tau in AD, but not in PSP and CBD. The lack of binding of ^{18}F-JNJ311 in the latter two tauopathies can most likely be explained by the ultrastructural differences, but also the different tau fractions that exist between these tauopathies and AD (*5*), which may significantly change JNJ311's binding site. Only one brain sample was, however, tested in the case of PSP and CBD. Another limitation of the PSP autoradiography study is the lower prevalence of tau inclusions in the frontal cortex, compared with the subthalamic nucleus, basal ganglia, or brain stem (*5*). A favorable pharmacokinetic profile is an important factor in the development of a PET tracer, but with a $\log D_{7.4}$ value of 2.2 and a polar surface area value of 51 Å^2, ^{18}F-JNJ311 has appropriate properties to efficiently pass the blood–brain barrier (*20*). This assumption was confirmed in the biodistribution studies in mice, because ^{18}F-JNJ311 displayed a moderate initial blood–brain barrier passage (SUVs of 1.9 at 2 min after injection). ^{18}F-JNJ311 also revealed a rapid brain washout (SUV of 0.1 at 60 min after injection). ^{18}F-JNJ311 displayed hereby a brain uptake and washout similar to ^{18}F-AV1451 (SUVs of 2.2 at 2 min after injection and 1.0 at 10 min after injection); this was demonstrated by the 2- to 60-min brain activity ratio, which was 30 for ^{18}F-JNJ311, higher than for ^{18}F-AV1451 (value of 18; $P < 0.05$), indicating a faster brain washout for ^{18}F-JNJ311 in mice. No pronounced bone uptake at 60 min after injection was also revealed in NMRI mice.

Further in vivo evaluation of ^{18}F-JNJ311 was done by performing small-animal PET studies in Wistar rats. Time–activity curves of the small-animal PET scans with ^{18}F-AV1451 show a brain uptake similar to those with ^{18}F-JNJ311 in rats. No noticeable influence on the brain time–activity curves was observed for self-blocking and self-displacement of ^{18}F-JNJ311 ($P > 0.05$ for all time points for) in rats, which indicates that there was no non–tau-related specific binding in the brain, in line with extensive CEREP and DiscoverX profiling (results in the preclinical in vitro characterization study (*12*)). On the other hand, lower brain uptake of ^{18}F-AV1451 was recorded during the baseline scan, compared with the pretreatment study ($P < 0.05$ at 5 min after injection). This effect may be explained by saturation of metabolic enzymes or plasma proteins leading to a higher free fraction of ^{18}F-AV1451 available for brain uptake. A similar effect was seen in the displacement study with ^{18}F-AV1451 ($P < 0.05$ at 38 min after injection). This possible interaction between the cold authentic reference compound AV1451 and ^{18}F-AV1451 may have consequences, because polypharmacy is common among AD patients

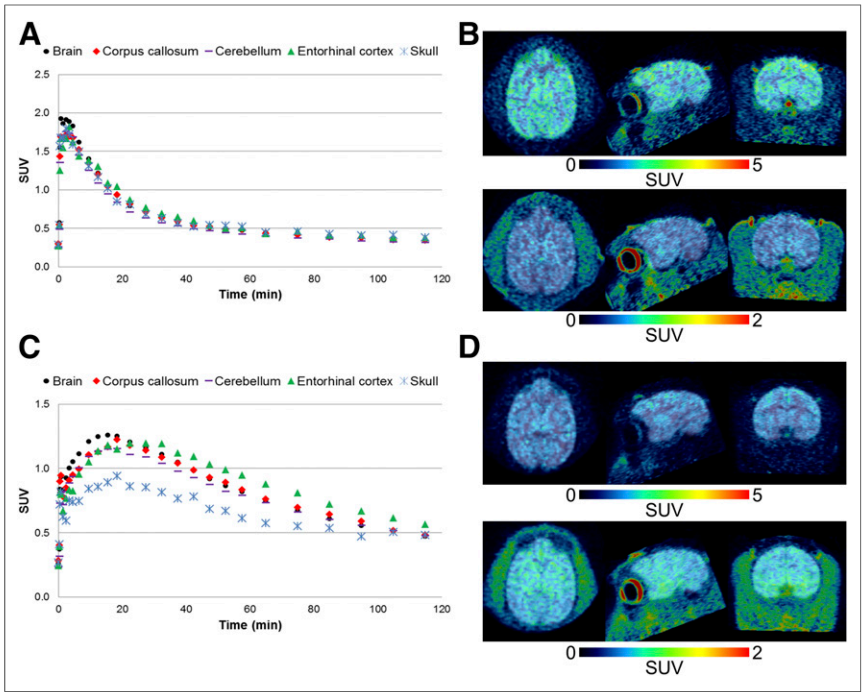

FIGURE 4. Small-animal PET time–activity curves for ^{18}F-JNJ311 (A) and ^{18}F-AV1451 (C) in whole brain, corpus callosum, cerebellum, enthorinal cortex, and skull of male rhesus monkey. Transversal, sagittal, and coronal images of baseline experiment with ^{18}F-JNJ311 (B) and ^{18}F-AV1451 (D): averaged image 1–10 min after tracer injection (top) and 60–120 min after tracer injection (bottom).

(*21*), and this may potentially lead to decreased plasma clearance of ^{18}F-AV1451. The influence of drugs on the metabolism of ^{18}F-AV1451 could therefore possibly complicate its PET quantification and theoretically lead to false conclusions.

Fast clearance from the brain, as seen in the latter biodistribution and small-animal PET studies with ^{18}F-JNJ311, could be explained by the rapid metabolism (and thus rapid plasma clearance) observed for ^{18}F-JNJ311 in the plasma of NMRI mice and the rhesus monkey (33% of intact tracer left 10 min after injection for mice and 35% of intact tracer left 30 min after injection for the monkey), with detection of one unidentified polar radiometabolite. This rapid plasma clearance was also seen in the human PK predictions for JNJ311 (Supplemental Table 1). The rate of metabolism was, however, considerably faster in mice than in the rhesus monkey (Supplemental Table 4). The detected radiometabolite was not able to pass the blood–brain barrier in mice, because the fraction of intact tracer remained high in brain homogenates over time (94% of intact tracer left at 60 min after injection). Similar findings were published for ^{18}F-AV1451 (*13*), with detection of one polar metabolite in plasma that also did not pass the blood–brain barrier in mice, although the rate of metabolism was not as pronounced as for ^{18}F-JNJ311 (84% of intact ^{18}F-AV1451 left at 10 min after injection).

The time–activity curves of both ^{18}F-JNJ311 and ^{18}F-AV1451 of the monkey small-animal PET study revealed a homogeneous distribution of both compounds in all brain regions, with no increased uptake in the corpus callosum. Time–activity curves of the skull, of ^{18}F-JNJ311 and ^{18}F-AV1451, showed that the focally increased uptake around the skull cannot be attributed to bone uptake, related to ^{18}F-fluoride, because the signal declines over time (Fig. 4). These areas of increased focal tracer uptake around the skull with the small-animal PET scan of ^{18}F-JNJ311 are probably related to fixation of an acrylic headpost to the skull of the monkey, used to position the head during MR scanning. This headpost can cause inflammation or scar formation of the skin around the headpost. Excessive binding of ^{18}F-fluoride in the skull could complicate quantification of ^{18}F-JNJ311 in the brain, because of partial-volume effects, for example, surrounding petrous bone spilling into the medial temporal cortex, but this bone uptake effect was thus seen only in rats and not in mice and the rhesus monkey. Because ^{18}F-AV1451 also showed significant bone uptake in rats, but not in mice and monkeys, both tracers seem susceptible to interspecies differences with regard to defluorination, as is the case for many PET tracers (*22,23*).

The superior brain pharmacokinetic profile of ^{18}F-JNJ311 led to the selection of this tracer as the optimal candidate for further tau PET exploration. Although ^{18}F-JNJ311 also seems to show a superior pharmacokinetic profile in rats and monkey compared with ^{18}F-AV1451, clinical PET scans with ^{18}F-JNJ311 in AD patients are necessary to make a relevant comparison. Human pharmacokinetic predictions for JNJ311 were made based on a mouse, rat, and dog PK study (0.25 mg/kg, JNJ311) and indicate a fast clearance in humans (Supplemental Table 1).

CONCLUSION

On the basis of its in vitro and in vivo preclinical profiling, ^{18}F-JNJ64349311 is a promising candidate for quantitative tau PET imaging in AD, with a favorable pharmacokinetic profile in comparison with the current benchmark ligands.

DISCLOSURE

This research was funded by Janssen Research and Development and the Institute for the Promotion of Innovation through Science and Technology in Flanders (IWT). No other potential conflict of interest relevant to this article was reported.

ACKNOWLEDGMENTS

We thank Julie Cornelis, Jana Hemelaers (Laboratory for Radiopharmacy, KU Leuven), and Christophe Ulens (Laboratory for Neuro- and Psychophysiology, KU Leuven) for their skillful help with the animal experiments. We also gratefully acknowledge the help of Astrid Bottelbergs and Ilse Lenaerts (Neuroscience Discovery, Janssen Research and Development, a division of Janssen Pharmaceutica NV, Beerse) with the immunohistochemistry and ^{3}H-autoradiography experiments. Finally, we express our appreciation for the scientific advice of Hartmuth Kolb (head of Neuroscience Biomarkers at Janssen Research and Development, LaJolla, USA).

REFERENCES

1. Cummings JL, Morstorf T, Zhong K. Alzheimer's disease drug-development pipeline: few candidates, frequent failures. *Alzheimers Res Ther.* 2014;6:37–44.
2. Lee VM, Goedert M, Trojanowski JQ. Neurodegenerative tauopathies. *Annu Rev Neurosci.* 2001;24:1121–1159.
3. Braak H, Braak E. Neuropathological stageing of Alzheimer-related changes. *Acta Neuropathol (Berl).* 1991;82:239–259.
4. Villemagne VL, Furumoto S, Fodero-Tavoletti M, et al. The challenges of tau imaging. *Future Neurol.* 2012;7:409–421.
5. Dani M, Brooks DJ, Edison P. Tau imaging in neurodegenerative diseases. *Eur J Nucl Med Mol Imaging.* 2016;43:1139–1150.
6. Schwarz AJ, Yu P, Miller BB, et al. Regional profiles of the candidate tau PET ligand ^{18}F-AV-1451 recapitulate key features of Braak histopathological stages. *Brain.* 2016;139:1539–1550.
7. Lowe VJ, Curran G, Fang P, et al. An autoradiographic evaluation of AV-1451 Tau PET in dementia. *Acta Neuropathol Commun.* 2016;4:58–77.
8. Chien DT, Bahri S, Szardenings AK, et al. Early clinical PET imaging results with the novel PHF-tau radioligand [F-18]-T807. *J Alzheimers Dis.* 2013;34:457–468.
9. Baker SL, Lockhart SN, Price JC, et al. Reference tissue-based kinetic evaluation of 18F-AV-1451 in aging and dementia. *J Nucl Med*. September 1, 2016 [Epub ahead of print].
10. Shcherbinin S, Schwarz AJ, Joshi A, et al. Kinetics of the tau PET tracer ^{18}F-AV-1451 (T807) in subjects with normal cognitive function, mild cognitive impairment, and Alzheimer disease. *J Nucl Med.* 2016;57:1535–1542.
11. Wooten D, Guehl NJ, Verwer EE, et al. Pharmacokinetic evaluation of the tau PET radiotracer [^{18}F]T807 ([^{18}F]AV-1451) in human subjects. *J Nucl Med.* 2017;58:484–491.
12. Rombouts FJ, Andres JI, Ariza M, et al. Discovery of N-(pyridin-4-yl)-1,5-naphthyridin-2-amines as potential tau pathology PET tracers for Alzheimer's disease. *J Med Chem.* 2017;60:1272–1291.
13. Declercq L, Celen S, Lecina J, et al. Comparison of new tau PET-tracer candidates with [^{18}F]T808 and [^{18}F]T807. *Mol Imaging.* 2016;15:1–15.
14. Gocan S, Cimpan G, Comer J. Lipophilicity measurements by liquid chromatography. *Adv Chromatogr.* 2006;44:79–176.
15. Xia CF, Arteaga J, Chen G, et al. [^{18}F]T807, a novel tau positron emission tomography imaging agent for Alzheimer's disease. *Alzheimers Dement.* 2013;9:666–676.
16. Casteels C, Vermaelen P, Nuyts J, et al. Construction and evaluation of multitracer small-animal PET probabilistic atlases for voxel-based functional mapping of the rat brain. *J Nucl Med.* 2006;47:1858–1866.
17. Van den Bergh A, Sinha V, Gilissen R, et al. Prediction of human oral plasma concentration-time profiles using preclinical data: comparative evaluation of prediction approaches in early pharmaceutical discovery. *Clin Pharmacokinet.* 2011;50:505–517.
18. Graff-Radford NR, Woodruff BK. Frontotemporal dementia. *Semin Neurol.* 2007;27:48–57.
19. Shah M, Catafau AM. Molecular imaging insights into neurodegeneration: focus on tau PET radiotracers. *J Nucl Med.* 2014;55:871–874.
20. Pike VW. PET radiotracers: crossing the blood-brain barrier and surviving metabolism. *Trends Pharmacol Sci.* 2009;30:431–440.
21. Singh S, Kushwah AS, Singh R, Farswan M, Kaur R. Current therapeutic strategy in Alzheimer's disease. *Eur Rev Med Pharmacol Sci.* 2012;16:1651–1664.
22. Celen S, Koole M, De AM, et al. Preclinical evaluation of ^{18}F-JNJ41510417 as a radioligand for PET imaging of phosphodiesterase-10A in the brain. *J Nucl Med.* 2010;51:1584–1591.
23. Sephton SM, Dennler P, Leutwiler DS, et al. Synthesis, radiolabelling and in vitro and in vivo evaluation of a novel fluorinated ABP688 derivative for the PET imaging of metabotropic glutamate receptor subtype 5. *Am J Nucl Med Mol Imaging.* 2012;2:14–28.